



Numerical solution of distributed-order time-fractional diffusion-wave equations using Laplace transforms



Christian Engström^{a,*}, Stefano Giani^b, Luka Grubišić^c

^a Department of Mathematics, Linnaeus University, 35195, Sweden

^b Department of Engineering, Durham University, South Rd, Durham, DH1 3LE, United Kingdom

^c Department of Mathematics, Faculty of Science, University of Zagreb, Bijenicka 30, Zagreb, 10000, Croatia

ARTICLE INFO

Article history:

Received 30 September 2022

Received in revised form 12 December 2022

MSC:

45K05

65N30

47G20

Keywords:

Numerical inverse Laplace transform

Fractional diffusion-wave equations

Numerical range

Resolvent estimates

ABSTRACT

In this paper, we consider the numerical inverse Laplace transform for distributed order time-fractional equations, where a discontinuous Galerkin scheme is used to discretize the problem in space. The success of Talbot's approach for the computation of the inverse Laplace transform depends critically on the problem's spectral properties and we present a method to numerically enclose the spectrum and compute resolvent estimates independent of the problem size. The new results are applied to time-fractional wave and diffusion-wave equations of distributed order.

© 2022 The Author(s). Published by Elsevier B.V. This is an open access article under the CC BY license (<http://creativecommons.org/licenses/by/4.0/>).

1. Introduction

Time-fractional equations are used to model anomalous phenomena in various fields, including diffusion and wave propagation [1,2]. Numerical methods for diffusion equations with a constant fractional order $0 < \beta < 1$ have been studied by many authors and common approaches include methods based on convolution quadrature [3] and the numerical inverse Laplace transform [4].

In recent years, wave equations with a constant fractional order $1 < \beta < 2$ [5,6] and distributed order fractional equations with $\beta \in [0, 2]$ have attracted great attention [5,7–11]. Distributed order fractional equations can be seen as a generalization of equations with a constant fractional order (or more generally a multi-term fractional order) in the sense that a constant order corresponds to a Dirac measure.

The Laplace transform is an important tool in the study of constant and distributed order fractional equations. The representation of the solution in terms of the inverse Laplace transform depends on a contour integration of the underlying operator function T . The spectrum of T is for $0 < \beta < 1$ easily enclosed and avoided in the contour integration. This is important since the common Talbot's approach for the numerical Laplace transform depends critically on the location of the spectrum and on the magnitude of the resolvent norm $\|T(s)^{-1}\|$ over the contour. In [12] the authors developed an approach to localize the spectrum and bound the resolvent norm for a (constant order) fractional viscoelastic beam equation.

In this paper, we study equations where the spectrum of the underlying operator function T is not easily enclosed. The approach to obtain spectral properties of T is based on numerical computations of an enclosure of the numerical range and

* Corresponding author.

E-mail address: christian.engstrom@lnu.se (C. Engström).

resolvent estimates for finite and infinite dimensional operator functions [13]. This knowledge is used to characterize the behavior of the inverse Laplace transform used to compute the solution of distributed-order time-fractional diffusion-wave equations at a given time t .

Assume that $f^{(n)}$ is an absolutely continuous function. Then, we define for $\beta > 0$ the Caputo fractional derivative as

$${}^C D_t^\beta f(t) = \frac{1}{\Gamma(n - \beta)} \int_0^t \frac{f^{(n)}(\tau)}{(t - \tau)^{\beta - n + 1}} d\tau, \quad (n - 1) < \beta < n.$$

The Caputo fractional derivative can be extended continuously to an operator mapping between larger function spaces and we refer to [14] for further details about ${}^C D_t^\beta$. In this paper, we consider distributed order time-fractional equations in the form

$$\int_0^2 \mathcal{W}(\beta) {}^C D_t^\beta u(x, t) d\beta + Au(x, t) = f(x, t), \quad (x, t) \in \Omega \times (0, T] \tag{1.1}$$

where \mathcal{W} is a real non-negative weight function and $(A, \text{dom } A)$ is a self-adjoint operator in the separable Hilbert space \mathcal{H} . In the numerical examples, we focus on the case when $A : L^2(\Omega) \rightarrow L^2(\Omega)$ for $\Omega \subset \mathbb{R}^2$ and $Au = u_{x_1 x_1} + u_{x_2 x_2}$.

R. Gorenflo, Y. Luchko, and M. Stojanović studied in [15] the Cauchy problem for a spatially one-dimensional distributed order time-fractional diffusion-wave equation with fractional order $\beta \in [0, 2]$. We consider numerical methods for the corresponding boundary problem in several spatial dimensions. The following three cases are studied:

The time-fractional diffusion equation

Assume that $\text{supp } \mathcal{W} \subset [0, 1]$. Then, the corresponding time-dependent problem is

$$\begin{cases} \int_0^1 \mathcal{W}(\beta) {}^C D_t^\beta u(x, t) d\beta + Au(x, t) = f(x, t), & (x, t) \in \Omega \times (0, T] \\ u(x, 0) = u_0(x), & x \in \Omega, \\ u(x, t) = 0, & (x, t) \in \partial\Omega \times (0, T]. \end{cases} \tag{1.2}$$

The time-fractional wave equation of distributed order

Assume that $\text{supp } \mathcal{W} \subset [1, 2]$. Then, the corresponding time-dependent problem is

$$\begin{cases} \int_1^2 \mathcal{W}(\beta) {}^C D_t^\beta u(x, t) d\beta + Au(x, t) = f(x, t), & (x, t) \in \Omega \times (0, T] \\ u(x, 0) = u_0(x), \quad u_t(x, 0) = u_1(x), & x \in \Omega, \\ u(x, t) = 0, & (x, t) \in \partial\Omega \times (0, T]. \end{cases} \tag{1.3}$$

The time-fractional diffusion-wave equation of distributed order

Assume that $\text{supp } \mathcal{W} \cap [0, 1]$ and $\text{supp } \mathcal{W} \cap [1, 2]$ are both non-empty. Then, the corresponding time-dependent problem is

$$\begin{cases} \int_0^2 \mathcal{W}(\beta) {}^C D_t^\beta u(x, t) d\beta + Au(x, t) = f(x, t), & (x, t) \in \Omega \times (0, T] \\ u(x, 0) = u_0(x), \quad u_t(x, 0) = u_1(x), & x \in \Omega, \\ u(x, t) = 0, & (x, t) \in \partial\Omega \times (0, T]. \end{cases} \tag{1.4}$$

Let $\hat{f}(s)$ denote the Laplace transform of $f(t)$. Then

$$\mathcal{L}\{{}^C D_t^\beta f\}(s) = s^\beta \hat{f}(s) - \sum_{k=0}^{n-1} s^{\beta-k-1} f^{(k)}(0) \quad (n - 1) < \beta < n.$$

The Laplace transform of (1.3) with respect to t is then

$$\int_1^2 \mathcal{W}(\beta) (s^\beta \hat{u}(x, s) - s^{\beta-1} u_0(x) - s^{\beta-2} u_1(x)) d\beta + A\hat{u}(x, s) = \hat{f}(x, s)$$

Set

$$m_p(s) = \int_1^2 \mathcal{W}(\beta) s^{\beta-p} d\beta, \quad p = 0, 1, 2.$$

With this notation, the problem after applying the Laplace transform with respect to time is

$$\hat{T}(s)\hat{u}(x, s) = m_1(s)u_0 + m_2(s)u_1 + \hat{f}(x, s), \quad \hat{T}(s) = m_0(s) + A.$$

The remainder of this paper is structured as follows. In Section 2, we study properties of the operator function \hat{T} and the corresponding operator functions for (1.2) and (1.4). In Section 3, we outline the used discontinuous Galerkin scheme and in Section 4, we consider the numerical computation of resolvent estimates. Lastly, in Section 5, several numerical test cases illustrate the theoretical results in the presiding sections.

2. Properties of the operator function

In this section, we study the operator function obtained after formally applying the Laplace transform to (1.1). Then

$$\hat{T}(s)\hat{u}(x, s) = \hat{F}(x, s), \quad \hat{T}(s) = m_0(s) + A,$$

where

$$m_0(s) = \int_0^2 \mathcal{W}(\beta) s^\beta d\beta$$

and \hat{F} is given by the source term and the initial condition(s) at time $t = 0$.

Let $\mathcal{L}(\mathcal{H})$ denote the collection of linear operators in the Hilbert space \mathcal{H} and take $\text{dom } \hat{T} = \text{dom } A$ as the domain, independently of $\lambda \in \mathcal{D}$. The operator function $\hat{T} : \mathcal{D} \rightarrow \mathcal{L}(\mathcal{H})$, with $\mathcal{D} \subset \mathbb{C}$, is then closed and the spectrum is defined as

$$\sigma(\hat{T}) = \{s \in \mathcal{D} : 0 \in \sigma(\hat{T}(s))\}.$$

The spectral properties are together with estimates of $\|\hat{T}(s)^{-1}\|$ of fundamental importance for determining the existence and behavior of the solution operator

$$T(t) = \frac{1}{2\pi i} \int_{\Gamma} e^{st} \hat{T}(s)^{-1} ds \tag{2.1}$$

for the time-dependent problem, [16].

2.1. An enclosure of the numerical range

The numerical range of $\hat{T} : \mathcal{D} \rightarrow \mathcal{L}(\mathcal{H})$ is the set

$$W(\hat{T}) = \{\lambda \in \mathcal{D} : \exists u \in \text{dom } \hat{T}, \|u\| = 1, \text{ so that } (\hat{T}(\lambda)u, u) = 0\},$$

where (\cdot, \cdot) and $\|\cdot\|$ denote the inner product and norm in \mathcal{H} , respectively. The numerical range of an operator function contains in general several components that can be bounded or unbounded. However, it is difficult to directly determine the properties of the numerical range. We will in this section consider a natural enclosure of the numerical range.

Take $u \in \text{dom } \hat{T}$, with $\|u\| = 1$ and set $\alpha_u = (Au, u)$. Then, $s \in W(\hat{T})$ if there exists a normalized vector $u \in \text{dom } \hat{T} \setminus \{0\}$ such that

$$t_{\alpha_u}(s) := m_0(s) + \alpha_u = 0.$$

One possible enclosure of $\overline{W(\hat{T})}$ is then

$$W_\alpha(\hat{T}) := \overline{\{s \in \mathcal{D} : t_\alpha(s) = 0, \alpha \in W(A)\}}, \quad t_\alpha(s) := m_0(s) + \alpha = 0.$$

In the following, we assume that $\mathcal{D} \subset \mathbb{C}$ is the maximal domain. As a convention we always use the principal value of the logarithmic function in all formulae.

Theorem 2.1. Assume that $\mathcal{W} \in L^\infty((0, 2))$ is a non-negative function with positive support, $\mu(\text{supp } \mathcal{W}) > c > 0$. Furthermore, the self-adjoint operator A is positive $A > a$, with $a > 0$. Then

1. $W_\alpha(\hat{T})$ is symmetric with respect to \mathbb{R} .
2. $W_\alpha(\hat{T}) \subset \{s \in \mathbb{C} : \text{Re } s < 0\}$.
3. $W_\alpha(\hat{T})$ is empty if $\text{supp } \mathcal{W} \subset [0, 1]$
4. Assume that $\text{supp } \mathcal{W} \subset [\beta_1, \beta_2] \subset (1, 2)$. Then $W_\alpha(\hat{T}) \cap S_{\beta_2}$ is empty, where

$$S_{\beta_2} = \{s = re^{i\beta} : -\pi/\beta_2 < \varphi < \pi/\beta_2, r > 0\}.$$

5. Assume that $\text{supp } \mathcal{W} \subset [\beta_1, \beta_2] \subset (1, 2)$ with $\beta_1 > \beta_2/2$. Then $W_\alpha(\hat{T}) \cap S_{\beta_1}$ is empty, where

$$S_{\beta_1} = \{s = re^{i\beta} : \pi/\beta_1 < |\varphi| \leq \pi, r > 0\}.$$

Proof. (1) By taking the real and imaginary parts, we conclude that s is a zero of t_α if and only if $t_\alpha(\bar{s}) = 0$.

(2) Assume that $t_\alpha(s) = 0$ for $s = re^{i\varphi}$, $0 \leq \varphi \leq \pi$. The imaginary and real parts of $t_\alpha(s) = 0$ are then

$$0 = \int_0^2 \mathcal{W}(\beta) e^{\beta \ln r} \sin(\beta\varphi) d\mu(\beta), \quad 0 = \int_0^2 \mathcal{W}(\beta) e^{\beta \ln r} \cos(\beta\varphi) d\mu(\beta) + \alpha.$$

Assume that $\text{supp } \mathcal{W} \cap [0, 1]$ or $\text{supp } \mathcal{W} \cap [1, 2]$ are non-empty. Take $\varphi = 0$. Then

$$\int_0^2 \mathcal{W}(\beta) e^{\beta \ln r} d\mu(\beta) + \alpha > a > 0.$$

Furthermore

$$\int_0^2 \mathcal{W}(\beta)e^{\beta \ln r} \sin(\beta\varphi)d\mu(\beta) > 0, \quad 0 < \varphi \leq \pi/2.$$

(3) Assume $\text{supp } \mathcal{W} \subset [0, 1]$. Take $0 < \varphi \leq \pi$. Then

$$\int_0^1 \mathcal{W}(\beta)e^{\beta \ln r} \sin(\beta\varphi)d\mu(\beta) > 0.$$

Hence, $W_\alpha(\hat{T})$ is empty.

(4) Assume $\text{supp } \mathcal{W} \subset [\beta_1, \beta_2]$ with $1 \leq \beta_1 < \beta_2 \leq 2$. Then,

$$\int_{\beta_1}^{\beta_2} \mathcal{W}(\beta)e^{\beta \ln r} \sin(\beta\varphi)d\mu(\beta) > 0, \quad 0 < \varphi \leq \pi/\beta_2.$$

Hence, $W_\alpha(\hat{T})$ in the upper half-plane belongs to the sector $\pi/\beta_2 < \varphi \leq \pi$.

(5) As in the proof of (4), but the integral is negative. \square

2.1.1. Approximation of the enclosure of the numerical range

Results of [Theorem 2.1](#) provide enclosures of the spectrum, which are essential for the numerical Laplace transform. In this subsection, we use numerical computations to obtain significantly tighter enclosures of the spectrum.

We base our method on classical results on the dependence of zeros of polynomials on perturbations in the coefficients of the polynomial. Such results have been used by Kato in his approach to the perturbation theory of eigenvalues of finite matrices [\[17\]](#). A more modern treatment, particularly suited to the setting of this paper, can be found in the book [\[18, Section 6.3\]](#).

Let us recall the main result from complex analysis, which will be the basis of our algorithm for the localization of the spectrum. Two roots of a function of a complex variable are called geometrically distinct if they are distinct points of \mathbb{C} . The dependence of roots of a collection of functions formally denoted by $z \mapsto f(z', z)$, $z' \in U' \subset \mathbb{C}^{n-1}$ on the parameter z' from the domain U' is described by the following result [\[18, Proposition 6.3.2\]](#), which, for completeness, we state in [Theorem 2.2](#).

Theorem 2.2. *Let $D \subset \mathbb{C}$ and $U' \subset \mathbb{C}^{n-1}$ be domains and let f be holomorphic on $U' \times D$. Assume that for given $m \in \mathbb{N}$ each of the functions $z \mapsto f(z', z)$, $z' \in U'$ has precisely m geometrically unique zeros. Then for each $z' \in U'$ there exists a neighborhood of z' in U' and m functions $s_i(\cdot)$, $i = 1, \dots, m$ that are holomorphic in the neighborhood such that*

$$f(z', z) = u(z', z) \prod_{j=1}^m (z - s_j(z'))^{k_j},$$

where k_i , $i = 1, \dots, m$ are positive integers and u is a non-vanishing holomorphic function.

We apply this result on our setting by recalling that $\alpha \in \mathcal{D} \subset \mathbb{C}$, and that $f(\alpha, s) := t_\alpha(s)$ is holomorphic in $\mathcal{D} \times \mathbb{C}$.

To turn this result into a practical algorithm, we will numerically approximate the enclosure of the numerical range by the generalized argument principle and continuation. The computation of zeros of complex functions by the evaluation of contour integrals is well known and we refer to [\[19\]](#) for details. The algorithm described above was implemented in the open-source software Chebfun [\[20\]](#) and it approximates the values of the contour integrals along the closed contour by expanding the integrand in a periodic Chebyshev series and then using the Clenshaw–Curtis rapidly converging quadrature.

Assume that t_α is holomorphic inside and on the closed contour γ and t_α has no zeros on γ . Then the argument principle implies

$$c_0(\alpha) := \frac{1}{2\pi i} \int_\gamma \frac{t_\alpha(s)}{t'_\alpha(s)} ds = \text{number of zeros inside } \gamma \tag{2.2}$$

Furthermore, if t_α has zeros $s_1(\alpha), s_2(\alpha), \dots, s_n(\alpha)$ inside γ , then the generalized argument principle implies

$$c_n(\alpha) := \frac{1}{2\pi i} \int_\gamma s^k \frac{t_\alpha(s)}{t'_\alpha(s)} ds = s_1(\alpha)^k + s_2(\alpha)^k + \dots + s_n(\alpha)^k \tag{2.3}$$

for higher moments of t_α .

In the numerical computations, we first fix $\alpha \in W(A)$ and use [\(2.2\)](#) to determine the number of zeros inside a circle. Then [\(2.3\)](#) is used to obtain all zeros, e.g. if there are two zeros then they are the roots of the polynomial

$$p_\alpha(z) = z^2 - c_1(\alpha)z + \frac{c_1(\alpha)^2 - c_2(\alpha)}{2}.$$

The roots can then be determined numerically.

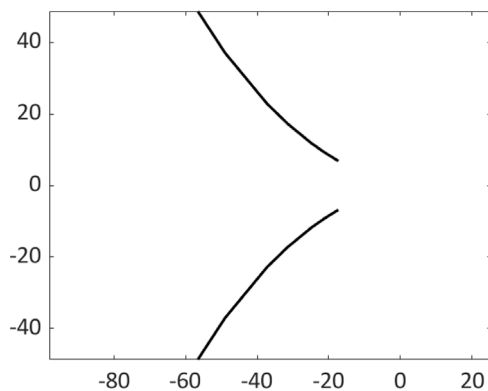


Fig. 1. The enclosure of the numerical range $W_\alpha(\hat{T})$ when $W(A) \subset [2\pi^2, \infty)$ truncated to a box in \mathbb{C} . The constants in (2.4) are $b_1 = 0.89/(\beta_2 - \beta_1)$, $b_2 = 0.1/(\beta_4 - \beta_3)$, $b_3 = 0.01/(\beta_6 - \beta_5)$ with $\beta_1 = 1, \beta_2 = 1.05, \beta_3 = 1.2, \beta_4 = 1.5, \beta_5 = 1.8, \beta_6 = 2$.

We note that the final procedure is a posteriori and heuristical, in that we first assess the number of geometrically unique zeros inside a contour using a quadrature, rather than exact integration. We then proceed and sample the parameter space \mathcal{D} in order to approximately localize the spectrum.

2.1.2. A case study of the piece-wise constant weight function

Given the fact that our algorithm provides an indicator for the enclosure of the numerical range, rather than a localization bound, we will now perform a more detailed analysis for the case of a piece-wise constant weight function \mathcal{W} . We note that several different weight functions have been considered in the literature [11,15].

Let first $1 \leq \beta_1 < \beta_2 < \dots < \beta_N \leq 2$ and

$$\mathcal{W}(\beta) = \sum_{j=1}^{N-1} b_j \chi_j(\beta), \quad \chi_j(\beta) = \begin{cases} 1, & \beta_j < \beta < \beta_{j+1}, \\ 0, & \text{otherwise.} \end{cases} \tag{2.4}$$

Assume $s \notin \{0, 1\}$. Then

$$\int_{\beta_1}^{\beta_2} s^\beta d\beta = \frac{s^{\beta_2} - s^{\beta_1}}{\log s},$$

where $\log s := \ln |s| + i \arg s$ with $-\pi < \arg s \leq \pi$. Then follows

$$m_0(s) := \sum_{j=1}^{N-1} b_j \int_{\beta_j}^{\beta_{j+1}} s^\beta d\beta = \sum_{j=1}^{N-1} b_j \frac{s^{\beta_{j+1}} - s^{\beta_j}}{\log s}. \tag{2.5}$$

Note that,

$$m_0(0) = 0, \quad m_0(1) = \sum_{j=1}^{N-1} b_j L_j,$$

where L_j denotes the length of the interval (β_j, β_{j+1}) . Fig. 1 presents numerical computations of $W_\alpha(\hat{T})$ for a case with three terms in the weight function (2.4). Below, we derive further properties of $W_\alpha(\hat{T})$ in the case when $N = 2$.

Let

$$m_0(s) = b_1 \frac{s^{\beta_2} - s^{\beta_1}}{\log s}, \tag{2.6}$$

and assume that $1 < \beta_1 < \beta_2 < 2$, where $\beta_1 > \beta_2/2$. Then $t_\alpha(s) = 0$ only if

$$b_1(s^{\beta_2} - s^{\beta_1}) + \alpha \log s = 0, \quad s = r e^{i\varphi}, \quad r > 0, \quad \pi/\beta_2 < \varphi < \pi/\beta_1.$$

Then we have a solution if

$$\begin{cases} b_1(r^{\beta_2} \cos \beta_2\varphi - r^{\beta_1} \cos \beta_1\varphi) + \alpha \ln r = 0, & (i) \\ b_1(r^{\beta_2} \sin \beta_2\varphi + r^{\beta_1} \sin \beta_1\varphi) + \alpha\varphi = 0. & (ii) \end{cases} \tag{2.7}$$

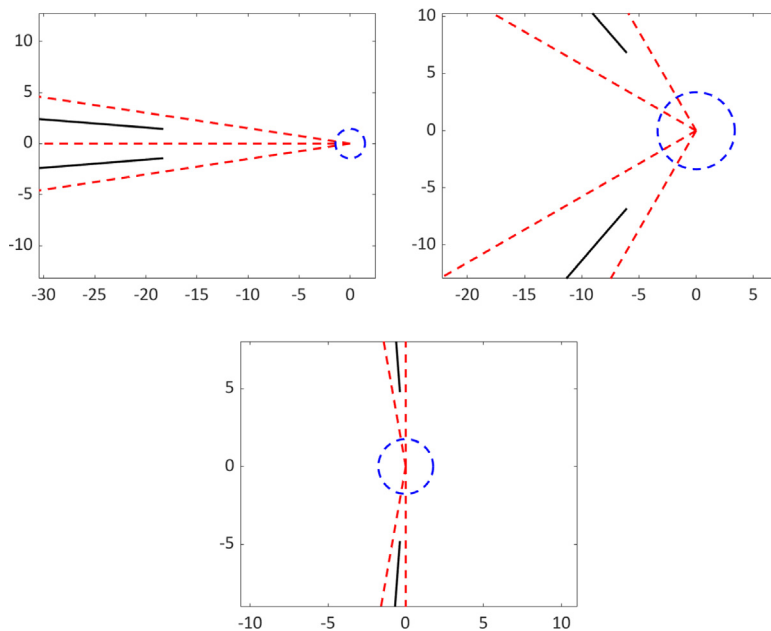


Fig. 2. The enclosure of the numerical range when $W(A) \subset [2\pi^2, \infty)$ and $b_1 = 1/(\beta_2 - \beta_1)$. Left: $\beta_1 = 1, \beta_2 = 1.05, r_0 = 1.44$. Middle: $\beta_1 = 1.2, \beta_2 = 1.5, r_0 = 3.37$. Right: $\beta_1 = 1.8, \beta_2 = 2, r_0 = 1.76$.

Assume that $r \leq 1$ and $\alpha > 2b_1\beta_2/\pi$: Then, the left hand side in (ii) is positive. Hence, $W_\alpha(\hat{T})$ does not intersect the unit disc $|s| < 1$. Moreover, $W_\alpha(\hat{T})$ does not intersect the disc with radius r_0 if

$$\frac{\alpha}{b_1} > \frac{2\beta_2 r_0^{\beta_2}}{\pi}. \tag{2.8}$$

Furthermore, the left side in (i) is positive if

$$\frac{\alpha}{b_1} \frac{\ln r}{r} > 2.$$

Numerical computations indicate that we have one geometrically unique zero in quadrant 2 and one in quadrant 3. According to [Theorem 2.2](#), the zeros should therefore change holomorphically (they will never come together).

[Fig. 2](#) illustrates the bounds for $N = 2$ in three different cases. In all sub-figures, the dotted disc contains no part of the numerical range. Moreover, the two dotted rays in the second quadrant bound one part of the numerical range and the two rays in the third quadrant bound the other part of the numerical range. The solid lines are numerically computed enclosures of the numerical range.

The support of \mathcal{W} is in the left figure close to one (almost diffusion). A more wave-like equation is illustrated in the middle figure and the result for a wave-like equation (β close to two) is depicted in the right figure.

3. Discretization of the Laplace operator and Fredholm functions

Assume that the positive self-adjoint operator A has a compact inverse and that m_0 is analytic. We consider then the operator function

$$\tilde{T}(s) := A^{-1/2} \hat{T}(s) A^{-1/2} = m_0(s)S + I, \quad S = A^{-1}, \tag{3.1}$$

which is an analytic Fredholm function of index zero. Hence, there can only be eigenvalue sequences with finite accumulation points at the boundary of \mathcal{D} [[21](#), [Theorem 8.92](#)]. Note that the results in [Section 2.1.1](#) imply that $\sigma(\hat{T})$ with [\(2.6\)](#) and domain $\mathcal{D} = \mathbb{C} \setminus \{0, 1\}$ cannot include branches of eigenvalues that accumulate to zero or one.

We will numerically consider the case when A is the Laplace operator. The spectral problem can then be reduced to an eigenvalue problem for the analytic Fredholm function [\(3.1\)](#).

3.1. Discontinuous Galerkin approximations for the Laplace operator

In the following, we outline the basic form of the symmetric interior penalty method (SIP) [[22](#)] for the Laplace eigenvalue problem [[23](#)] on a bounded and regular domain $\Omega \subset \mathbb{R}^2$. Let \mathcal{V}_h^p denote the space of piece-wise polynomials of degree p on a conforming shape-regular triangulation \mathcal{T}_h of Ω .

Moreover, \mathcal{E} and \mathcal{E}_i denote the set of all edges of \mathcal{T}_h and the set of just the internal edges, respectively. Assume that $K_1, K_2 \in \mathcal{T}_h$ share an edge $e \subset \partial K_1 \cap \partial K_2$ and let n_1, n_2 denote the outward pointing normals on the edge. The averages $\{\cdot\}$ and jumps $[\cdot]$ of a piece-wise smooth function w on $K_1 \cup K_2$ are then defined as

$$\begin{aligned} \{\{w\}\} &= \frac{1}{2}(w_1 + w_2), \quad [[w]] = w_1 n_1 + w_2 n_2, \\ \{\{\nabla w\}\} &= \frac{1}{2}(\nabla w_1 + \nabla w_2), \quad [[\nabla w]] = \nabla w_1 \cdot n_1 + \nabla w_2 \cdot n_2, \end{aligned}$$

By w_i , we denote the traces of w on e taken from within the interior of K_i , respectively.

On boundary edges, we set $\{\{\nabla w\}\} = \nabla w$ and $[[w]] = wn$, with n denoting the unit outward normal vector on the boundary $\partial\Omega$.

The symmetric interior penalty bilinear form $a^h : \mathcal{V}_h^p \times \mathcal{V}_h^p \rightarrow \mathbb{R}$ is given by

$$\begin{aligned} a^h[u^h, v^h] &= (\nabla u^h, \nabla v^h)_{\mathcal{T}_h} - (\{\{\nabla u^h\}\}, [[v^h]])_{\mathcal{E}} - (\{\{\nabla v^h\}\}, [[u^h]])_{\mathcal{E}} \\ &\quad + \sum_{e \in \mathcal{E}} \zeta \frac{p^2}{h_e} ([[u^h]], [[v^h]])_e, \end{aligned} \tag{3.2}$$

where h_e is the length of the edge e and where ζ is the penalty parameter. The bilinear form a^h is continuous and coercive for a value of ζ large enough [24].

The discrete eigenvalue problem for the Laplace operator then reads: find $(\mu^h, u^h) \in \mathbb{R} \times \mathcal{V}_h^p$ such that

$$a^h[u^h, v^h] = \mu^h(u^h, v^h)$$

holds for all $v^h \in \mathcal{V}_h^p$.

3.2. Discontinuous Galerkin approximations for the source problems

We solve the equation $\hat{T}(s)\hat{u} = h$ numerically for $s \in \Gamma$. Consider the \hat{T} in Fig. 2 (left) when $t = 1$. Note that Fig. 2 shows that the inverse $\hat{T}(s)^{-1}$ exists inside the circle. Take 32 quadrature nodes on Γ and compute $m_0(s)$ for those nodes. The function-values $m_0(s)$ with the largest positive real parts and the largest negative real parts are then $0.2381 \pm 0.1832i$ and $-38.5372 \pm 1.0422i$, respectively. Since $m_0(s) \in \mathbb{C}$, the source problem is posed on the complex plane and it has the form:

$$a^h[u^h, v^h] + m_0(s)(u^h, v^h)_{\mathcal{T}_h} = (h, v^h)_{\mathcal{T}_h}, \tag{3.3}$$

in contrast to Eq. (3.2), here, the inner products in the definition of the problem and inside the bilinear form a^h are the inner product of the space $L^2(\Omega)$ on \mathbb{C} , i.e.

$$(u, v)_S := \int_S u \bar{v} \, d\mathbf{x}.$$

By definition, problem (3.3) is elliptic and Hermitian and can be solved with similar methods used for real and symmetric elliptic problems.

4. Computation of resolvent estimates

Let $\sigma^\epsilon(\hat{T})$ denote the ϵ -pseudospectrum

$$\sigma^\epsilon(\hat{T}) := \{s \in \mathcal{D} : \exists u \in \text{dom } \hat{T}, \|u\| = 1, \text{ so that } \|\hat{T}(s)u\| < \epsilon\}. \tag{4.1}$$

Assume that $s \in \sigma^\epsilon(\hat{T}) \setminus \sigma(\hat{T})$. Then there is a vector $u \in \text{dom } \hat{T}$, $\|u\| = 1$ such that

$$\epsilon > \|\hat{T}(s)u\| \geq |(\hat{T}(s)u, u)| = |t_{\alpha u}(s)|.$$

Hence, the set

$$W_\alpha^\epsilon(\hat{T}) = W_\alpha(\hat{T}) \cup \{s \in \mathcal{D} \setminus W_\alpha(\hat{T}) : \exists \alpha \in W(A) \text{ so that } t_\alpha(s) < \epsilon\}.$$

is an enclosure of $\sigma^\epsilon(T)$. Importantly, $W_\alpha^\epsilon(\hat{T})$ is explicitly computable. The enclosure of the ϵ - numerical range $W_\alpha^\epsilon(\hat{T})$ was introduced in [13] and applied to rational operator functions in [25,26].

Assume that the positive self-adjoint operator A has compact resolvent and that m_0 is analytic. Then, we consider the operator function (3.1) and the corresponding matrix-valued function

$$\tilde{T}_h(s) := A_h^{-1/2} \hat{T}_h(s) A_h^{-1/2} = m_0(s) S_h + I_h, \quad S = A_h^{-1/2} M_h A_h^{-1/2}.$$

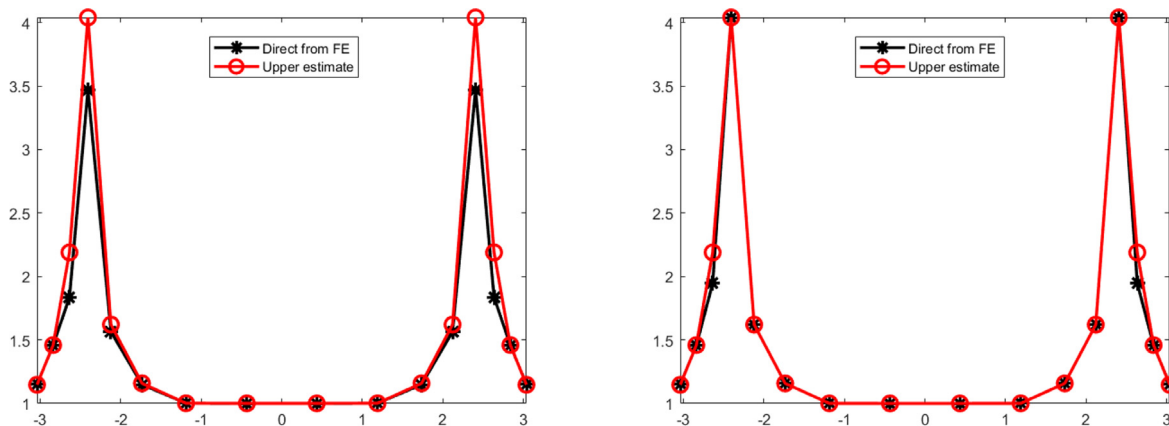


Fig. 3. Upper estimation of the resolvent norm and computation based on FE matrices. Left: $p = 1$ (dofs = 108). Right: $p = 8$ (dofs = 1620).

The solution operator (2.1) depends on the integration curve Γ . We will compute $W_\alpha^\epsilon(\tilde{T})$ and (4.1) along the integration curve used to solve the time-dependent problems, where the enclosure is obtained from the zeros of

$$t_\alpha(s) = m_0(s)\alpha + 1, \quad \alpha \in W(S).$$

Fig. 3 depicts the upper bound on $\|\tilde{T}_h(s)^{-1}\|$, $s \in \Gamma_{0.4}^h$ when $\beta_1 = 1.8$, $\beta_2 = 2$, $b_1 = 1/(\beta_2 - \beta_1)$, $\alpha \in [0, 1/\lambda_1]$, where $\lambda_1 = 2\pi^2$ is the lowest eigenvalue of the Dirichlet Laplace operator when Ω is the unit square (the values at the quadrature nodes are marked by red circles). Moreover, an estimate of the resolvent norm for two Galerkin approximations of the problem $\|\tilde{T}(s)^{-1}\|$, $s \in \Gamma_{0.4}^h$, $\alpha \in [1/\lambda_{\max}^h, 1/\lambda_1^h]$ is depicted in the same figures (the values at the quadrature nodes are marked by black stars).

5. Numerical solution of distributed-order time-fractional equations

Under suitable conditions on Γ and the data, a classical solution of (1.2), (1.3), or (1.4) can be represented in the form

$$u(t) = \frac{1}{2\pi i} \int_\Gamma e^{st} \hat{T}(s)^{-1} h(s) ds, \quad h(s) = h_0(s) + \hat{f}(s),$$

or

$$u(t) = \frac{1}{2\pi i} \int_\Gamma e^{st} \hat{T}(s)^{-1} h_0(s) ds + \frac{1}{2\pi i} \int_\Gamma \hat{T}(s)^{-1} \int_0^t e^{s(t-\tau)} f(\tau) d\tau ds. \tag{5.1}$$

The function h_0 is for the time-fractional diffusion equation of distributed order in (1.2) given by

$$h_0(s) = m_1(s)u_0, \quad m_1(s) = \int_0^1 \mathcal{W}(\beta) s^{\beta-1} d\beta.$$

This case is extensively studied [2,7] and therefore not the focus of this paper. The function h_0 is for the time-fractional wave equation of distributed order in (1.4) given by

$$h_0(s) = m_1(s)u_0 + m_2(s)u_1, \quad m_p(s) = \int_1^2 \mathcal{W}(\beta) s^{\beta-p} d\beta, \quad p = 1, 2.$$

Previous studies of this problem include [5,7,9].

The function h_0 is for the time-fractional diffusion-wave equation of distributed order in (1.4) given by

$$h_0(s) = m_1(s)u_0 + m_2(s)u_1, \quad m_p(s) = \int_0^2 \mathcal{W}(\beta) s^{\beta-p} d\beta, \quad p = 1, 2.$$

The mathematical analysis for this problem has started but is still in its infancy [15].

The optimal constants in several different contours Γ have been determined for a few parabolic problems [27]. The optimal contour will in our cases depend on the used weight function \mathcal{W} . Another common approach for computing contour integrals is to use higher than double precision [28]. However, optimization of the contour for a given \mathcal{W} or using high precision computations is beyond the scope of this paper.

In the following, we focus on illustrating the theoretical results in the previous sections. It is then sufficient to use the contour in [27] and standard double precision.

Consider Talbot’s contour parameterized by

$$s(\alpha) = \sigma_0 + \mu(\alpha \cot \alpha + v i \alpha), \quad -\pi < \alpha < \pi,$$

where $\sigma_0 + \mu > \max \operatorname{Re} \sigma(\hat{T}_h)$ and u can be represented as

$$u(t) = \frac{1}{2\pi i} \int_{-\pi}^{\pi} e^{s(\alpha)t} s'(\alpha) \hat{T}_h^{-1}(s(\alpha)) h(s(\alpha)) d\alpha. \tag{5.2}$$

The representation (5.1) is the same but we also need to evaluate the integration in the second term numerically.

5.1. Test cases with the discontinuous Galerkin approximation

For simplicity, we restrict the numerical computations to $\Omega = (0, 1)^2$. The solution is based on (5.1) and the vectorized adaptive quadrature implemented in the MATLAB function *integral*.

In all test cases, we used a course mesh and $p = 8$, which result in finite element matrices of size 1620. Furthermore, 128 quadrature nodes are used in the approximation of the inverse Laplace transform. The source term f is chosen such the exact solution can be written in the form

$$u(x_1, x_2, t) = \sin(\pi x_1) \sin(\pi x_2)(t^3 + 1), \tag{5.3}$$

or

$$u(x_1, x_2, t) = \arctan(x_1) \sin(\pi x_1) \sin(2\pi x_2)(t^3 + 1). \tag{5.4}$$

The solution in (5.4) oscillates more rapidly compared to (5.3) and it decreases fast when $x_1 \rightarrow 0$. Hence, with the considered uniform h and p distribution, we expect a considerably larger error for the problem with the solution (5.4) compared to (5.3). The main focus of the numerical simulations is to further illustrate the enclosure of the numerical range and a scaled Talbot’s contour for different cases.

A polynomial dependence on time t is often used in test cases for distributed time-fractional equations [5,7,9]. Only small values on time ($t < 1$) are usually considered since the solutions grow with t . However, we will for illustration purposes also consider larger values of t . The weight function \mathcal{W} is in all test cases

$$\mathcal{W}(\beta) = b_1 \chi_1(\beta), \quad \chi_1(\beta) = \begin{cases} 1, & \beta_1 < \beta < \beta_2, \\ 0, & \text{otherwise} \end{cases} \tag{5.5}$$

and we consider test cases of time-fractional wave Eqs. (1.3) and diffusion-wave Eqs. (1.4) of distributed order. In the computation of the source term

$$f(x, t) = \int_0^2 \mathcal{W}(\beta) {}^C D_t^\beta u(x, t) d\beta + Au(x, t)$$

we use that

$${}^C D_t^\beta t^\alpha = \frac{\Gamma(\alpha + 1)}{\Gamma(\alpha - \beta + 1)} t^{\alpha - \beta}, \quad n - 1 < \beta < n, \quad \alpha > n - 1,$$

and

$${}^C D_t^\beta t^\alpha = 0, \quad n - 1 < \beta < n, \quad \alpha \leq n - 1, \quad \alpha \in \mathbb{N}.$$

The integral in the definition of f is then computed using the MATLAB function *integral*. A numerical evaluation of f is necessary in most cases, except for some special cases with e.g. a Gamma function as a weight function (since the fractional derivative of a polynomial contains the Gamma function). In this paper, we:

1. Compute the smallest and largest eigenvalue of A_h .
2. Compute the enclosure of the numerical range of \hat{T}_h .
3. Check if the standard contour crosses the enclosure.
4. Compute the resolvent estimate for the considered values of t .
5. Check the error in the solution for two test cases (5.3) and (5.4).

Note that we only need an estimate of the numerical range of the matrix A_h . The use of these estimates does not depend on the quality of the approximation of the eigenvalues of the Dirichlet Laplace operator by the eigenvalues of A_h . Moreover, t_α depends for large α smoothly on α . Therefore, for fine discretizations we can use ∞ as an upper estimate on $W(A_h)$.

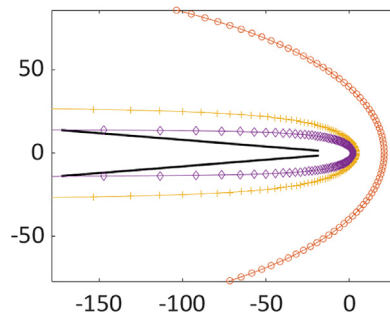


Fig. 4. The constants in (5.5) are $b_1 = 1/(\beta_2 - \beta_1)$, $\beta_1 = 1$, $\beta_2 = 1.05$. The two solid black lines depict the enclosure of the numerical range. The remaining curves are, counting from the right to left, Γ_1 , Γ_5 , and Γ_{10} .

Table 1
 $\beta_1 = 1, \beta_2 = 1.05, b_1 = 1/(\beta_2 - \beta_1)$.

L_2 -error	(5.3)	(5.4)
$t = 1$	$1.3e-05$	$1.5e-03$
$t = 5$	$8.2e-06$	$9.0e-03$
$t = 10$	$1.5e-05$	$4.5e-02$

5.2. Almost diffusion equation

Consider the time-fractional wave Eq. (1.3) with $\beta_1 = 1$ and $\beta_2 = 1.05$. Let $-A_h$ denote the discretization of the Laplace operator and compute numerically its lowest and largest eigenvalues. Then, we obtain the numerical range $W(A_h) = [19.73, 4.27 \cdot 10^5]$. The enclosure of the numerical range $W_\alpha(\hat{T}_h)$ is for the given $W(A_h)$ computed numerically using the approach in Section 2.1.1. The two solid black lines in Fig. 4 depict the numerically computed enclosure of the numerical range. The remaining curves in the figure are, counting from right to left, Γ_1 , Γ_5 , and Γ_{10} . The contour Γ_t will for larger values of t cross the enclosure of the numerical range.

It is for the computation of the inverse Laplace transform also important that the norm of the resolvent is not too large. The resolvent estimates are computed along Γ_t using the approach in Section 4. For given Γ_t this results in the set

$$\hat{W}_\alpha^\epsilon(\tilde{T}_h) = \{s \in \Gamma_t : \exists \alpha \in W(A_h) \text{ so that } t_\alpha(s) < \epsilon\}.$$

Finally, we take the maximum over the considered contours and obtain

$$\max_{t \in \{1, 5, 10\}} \max_{s \in \Gamma_t(s)} \|\tilde{T}_h(s)^{-1}\| \leq 0.42.$$

Note that this computation only requires the lowest and largest eigenvalue of A_h and the same approach can be used in the infinite-dimensional case [13].

In Table 1, we present relative L_2 -errors when the exact solutions are (5.3) and (5.4). The errors are, as expected, considerably larger for the problem with the less smooth solution (5.4) compared to (5.3).

5.3. Wavelike equation I

Consider the time-fractional wave Eq. (1.3) with $\beta_1 = 1.2$ and $\beta_2 = 1.5$, which is a more wavelike equation compared to the problem in Section 5.2. We use the same discretization as in the previous test case and compute the enclosure of the numerical range $W_\alpha(\hat{T}_h)$ numerically using the approach in Section 2.1.1. The two solid black lines in Fig. 5 depict the numerically computed enclosure of the numerical range and the remaining curves in the figure are, counting from right to left, $\Gamma_{0.125}$, $\Gamma_{0.25}$, and $\Gamma_{0.4}$. The contour Γ_t will for larger values of t cross the enclosure of the numerical range. Hence, a different contour should in general be used for larger values of t . However, note that the term $e^{s(\alpha)t}$ in the inverse Laplace transform is very small when $-\text{Re } s(\alpha) \gg 1$. Hence, the accuracy in the solution may be good also for larger values of t . Moreover, the accuracy of the solution will depend on the oscillations in the data [29].

The resolvent estimates are as in Section 2.1.1 computed along Γ_t using the approach from Section 4. The maximum of the norm of the resolvent is

$$\max_{t \in \{0.125, 0.25, 0.4\}} \max_{s \in \Gamma_t(s)} \|\tilde{T}_h(s)^{-1}\| \leq 0.049$$

In Table 2, we present relative L_2 -errors when the exact solutions are solution are (5.3) and (5.4). The errors are, as expected considerably larger for the problem with the less smooth solution (5.4) compared to (5.3).

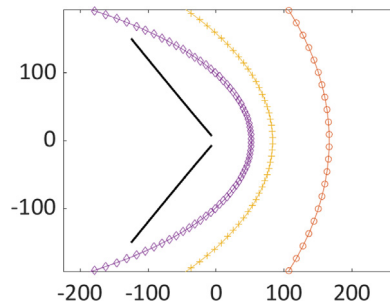


Fig. 5. The constants in (5.5) are $b_1 = 1/(\beta_2 - \beta_1)$, $\beta_1 = 1.2$, $\beta_2 = 1.5$. The two solid black lines depict the enclosure of the numerical range. The remaining curves are, counting from the right to left, $\Gamma_{0.125}$, $\Gamma_{0.25}$, and $\Gamma_{0.4}$.

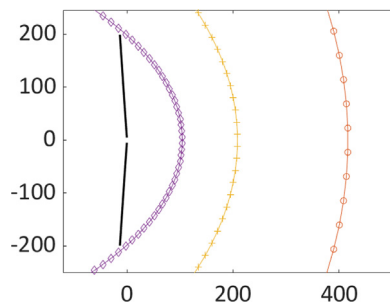


Fig. 6. The constants in (5.5) are $b_1 = 1/(\beta_2 - \beta_1)$, $\beta_1 = 1.8$, $\beta_2 = 2$. The two solid black lines depict the enclosure of the numerical range. The remaining curves are, counting from the right to left, $\Gamma_{0.05}$, $\Gamma_{0.1}$, and $\Gamma_{0.2}$.

Table 2
 $\beta_1 = 1.2$, $\beta_2 = 1.5$, $b_1 = 1/(\beta_2 - \beta_1)$.

L_2 -error	(5.3)	(5.4)
$t = 0.125$	$6.4e-07$	$1.1e-04$
$t = 0.25$	$5.3e-07$	$4.3e-04$
$t = 0.4$	$1.1e-06$	$1.0e-03$

Table 3
 $\beta_1 = 1.8$, $\beta_2 = 2$, $b_1 = 1/(\beta_2 - \beta_1)$.

L_2 -error	(5.3)	(5.4)
$t = 0.05$	$8.3e-08$	$9.3e-08$
$t = 0.1$	$7.1e-08$	$7.3e-06$
$t = 0.2$	$2.6e-07$	$2.4e-05$

5.4. Wavelike equation II

Consider the time-fractional wave Eq. (1.3) with $\beta_1 = 1.8$ and $\beta_2 = 2$, which is a wave-like equation. Hence, we expect that the spectrum of T is close to the imaginary axis. We use the same discretization as in the previous test cases and compute the enclosure of the numerical range $W_\alpha(\tilde{T}_h)$ numerically using the approach in Section 2.1.1. The two solid black lines in Fig. 6 depict the numerically computed enclosure of the numerical range and the remaining curves in the figure are, counting from right to left, $\Gamma_{0.05}$, $\Gamma_{0.1}$, and $\Gamma_{0.2}$.

The resolvent estimates are as in Section 2.1.1 computed along Γ_t using the approach from Section 4. The maximum of the norm of the resolvent is

$$\max_{t \in \{0.05, 0.1, 0.2\}} \max_{s \in \Gamma_t(s)} \|\tilde{T}_h(s)^{-1}\| \leq 0.0026.$$

In Table 3, we present relative L_2 -errors when the exact solutions are (5.3) and (5.4).

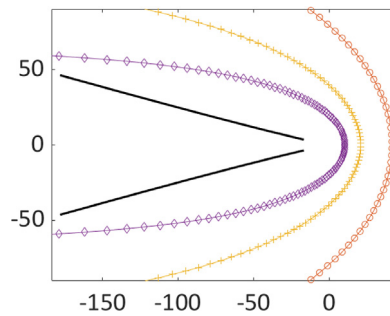


Fig. 7. The constants in (5.5) are $b_1 = 1/(\beta_2 - \beta_1)$, $\beta_1 = 0.9$, $\beta_2 = 1.2$. The two solid black lines depict the enclosure of the numerical range. The remaining curves are, counting from the right to left, $\Gamma_{0.5}$, Γ_1 , and Γ_2 .

Table 4
 $\hat{\beta}_1 = 0.9, \hat{\beta}_2 = 1, \beta_1 = 1, \beta_2 = 1.2, b_1 = 1/(\beta_2 - \hat{\beta}_1)$.

L_2 -error	(5.3)	(5.4)
$t = 0.5$	$5.0e-07$	$1.7e-03$
$t = 1$	$4.3e-06$	$3.7e-03$
$t = 2$	$8.0e-06$	$1.1e-02$

5.5. Diffusion-wave equation

In the last example, we consider the time-fractional diffusion-wave equation of distributed order (1.4). Assume that

$$\text{supp } \mathcal{W} \cap [0, 1] \subset [\hat{\beta}_1, \hat{\beta}_2], \quad \text{supp } \mathcal{W} \cap [1, 2] \subset [\beta_1, \beta_2]$$

are both non-empty with respect to the Lebesgue measure. Then it follows from Theorem 2.1(3) and (4) that $W_\alpha(\hat{T}) \cap S_{\beta_2}$ is empty, where

$$S_{\beta_2} = \{s = re^{i\beta} : -\pi/\beta_2 < \varphi \leq \pi/\beta_2, r > 0\}.$$

Take $\hat{\beta}_1 = 0.9, \hat{\beta}_2 = 1, \beta_1 = 1, \beta_2 = 1.2, b_1 = 1/(\beta_2 - \hat{\beta}_1)$. We use the same discretization as in the previous test cases and compute the enclosure of the numerical range $W_\alpha(\hat{T}_h)$ numerically using the approach in Section 2.1.1. The two solid black lines in Fig. 7 depict the numerically computed enclosure of the numerical range and the remaining curves in the figure are, counting from right to left, $\Gamma_{0.5}$, Γ_1 , and Γ_2 .

The resolvent estimates are as in Section 2.1.1 computed along Γ_t using the approach 4. The maximum of the norm of the resolvent is

$$\max_{t \in \{0.5, 1, 2\}} \max_{s \in \Gamma_t(s)} \|\tilde{T}_h(s)^{-1}\| \leq 0.26.$$

In Table 4, we present relative L_2 -errors when the exact solutions are (5.3) and (5.4). The errors are, as in previous test cases, considerably larger for the problem with the less smooth solution (5.4) compared to (5.3).

6. Conclusions

We have presented a numerical method to approximate an enclosure of the numerical range of a class of operator functions. The new results are applied to distributed-order time-fractional equations and we use an approach based on the numerical inverse Laplace transform and a discontinuous Galerkin scheme to numerically approximate the solution. The symmetric interior penalty method is used to illustrate the results but the proposed method is independent of the scheme used to discretize the operator A .

Data availability

Data will be made available on request.

Acknowledgments

LG was supported by the Hrvatska Zaklada za Znanost (Croatian Science Foundation) under the grant IP-2019-04-6268 -Randomized low-rank algorithms and applications to parameter dependent problems. CE was supported by the Swedish Research Council under Grant No. 2021-04537.

References

- [1] Francesco Mainardi, *Fractional Calculus and Waves in Linear Viscoelasticity*, Imperial College Press, London, 2010, p. xx+347, An introduction to mathematical models.
- [2] Bangti Jin, *Fractional Differential Equations—An Approach via Fractional Derivatives*, in: *Applied Mathematical Sciences*, vol. 206, Springer, Cham, 2021, p. xiv+368, ©2021.
- [3] Eduardo Cuesta, Christian Lubich, Cesar Palencia, Convolution quadrature time discretization of fractional diffusion-wave equations, *Math. Comp.* 75 (254) (2006) 673–696.
- [4] William Mclean, Vidar Thomée, Numerical solution via Laplace transforms of a fractional order evolution equation, *J. Integral Equations Appl.* 22 (1) (2010) 57–94.
- [5] H. Ye, F. Liu, V. Anh, Compact difference scheme for distributed-order time-fractional diffusion-wave equation on bounded domains, *J. Comput. Phys.* 298 (2015) 652–660.
- [6] Caixia Ou, Dakang Cen, Seakweng Vong, Zhibo Wang, Mathematical analysis and numerical methods for Caputo-Hadamard fractional diffusion-wave equations, *Appl. Numer. Math.* 177 (2022) 34–57.
- [7] Hadi Mohammadi-Firouzjaei, Hojatollah Adibi, Mehdi Dehghan, Local discontinuous Galerkin method for distributed-order time-fractional diffusion-wave equation: application of Laplace transform, *Math. Methods Appl. Sci.* 44 (6) (2021) 4923–4937.
- [8] Armando Consiglio, Francesco Mainardi, On the evolution of fractional diffusive waves, *Ric. Mat.* 70 (1) (2021) 21–33.
- [9] Xiaoli Li, Hongxing Rui, A block-centered finite difference method for the distributed-order time-fractional diffusion-wave equation, *Appl. Numer. Math.* 131 (2018) 123–139.
- [10] Mehdi Dehghan, Mostafa Abbaszadeh, A Legendre spectral element method (SEM) based on the modified bases for solving neutral delay distributed-order fractional damped diffusion-wave equation, *Math. Methods Appl. Sci.* 41 (9) (2018) 3476–3494.
- [11] Guang-hua Gao, Zhi-zhong Sun, Two alternating direction implicit difference schemes for solving the two-dimensional time distributed-order wave equations, *J. Sci. Comput.* 69 (2) (2016) 506–531.
- [12] Matthew J. Colbrook, Lorna J. Ayton, A contour method for time-fractional PDEs and an application to fractional viscoelastic beam equations, *J. Comput. Phys.* 454 (2022) Paper No. 110995, 24.
- [13] Christian Engström, Axel Torshage, Enclosure of the numerical range of a class of non-selfadjoint rational operator functions, *Integral Equations Operator Theory* 88 (2) (2017) 151–184.
- [14] Bangti Jin, Raytcho Lazarov, Joseph Pasciak, William Rundell, Variational formulation of problems involving fractional order differential operators, *Math. Comp.* 84 (296) (2015) 2665–2700.
- [15] Rudolf Gorenflo, Yuri Luchko, Mirjana Stojanović, Fundamental solution of a distributed order time-fractional diffusion-wave equation as probability density, *Fract. Calc. Appl. Anal.* 16 (2) (2013) 297–316.
- [16] Jan Prüß, *Evolutionary Integral Equations and Applications*, in: *Monographs in Mathematics*, vol. 87, Birkhäuser Verlag, Basel, 1993, p. xxvi+366.
- [17] T. Kato, *Perturbation Theory for Linear Operators*, in: *Classics in Mathematics*, Springer Berlin Heidelberg, 1995.
- [18] J. Lebl, *Tasty Bits of Several Complex Variables*, Lulu.com, 2016.
- [19] Anthony P. Austin, Peter Kravanja, Lloyd N. Trefethen, Numerical algorithms based on analytic function values at roots of unity, *SIAM J. Numer. Anal.* 52 (4) (2014) 1795–1821.
- [20] Tobin A. Driscoll, Nicholas Hale, Lloyd N. Trefethen, *Chebfun Guide*, Pafnuty Publications, Oxford, 2014.
- [21] Michael Renardy, Robert C. Rogers, *An Introduction to Partial Differential Equations*, second ed., in: *Texts in Applied Mathematics*, vol. 13, Springer-Verlag, New York, 2004, p. xiv+434.
- [22] D. Arnold, F. Brezzi, B. Cockburn, L. Marini, Unified analysis of discontinuous Galerkin methods for elliptic problems, *SIAM J. Numer. Anal.* 39 (5) (2002) 1749–1779.
- [23] Stefano Giani, Luka Grubišić, Jeffrey S. Owall, Benchmark results for testing adaptive finite element eigenvalue procedures, *Appl. Numer. Math.* 62 (2) (2012) 121–140.
- [24] S. Prudhomme, F. Pascal, J.T. Oden, A. Romkes, Review of a Priori Error Estimation for Discontinuous Galerkin Methods, TICAM REPORT 00-27, The University of Texas at Austin.
- [25] Christian Engström, Axel Torshage, Accumulation of complex eigenvalues of a class of analytic operator functions, *J. Funct. Anal.* 275 (2) (2018) 442–477.
- [26] Christian Engström, Axel Torshage, Spectral properties of conservative, dispersive, and absorptive photonic crystals, *GAMM-Mitt.* 41 (3) (2018) e201800009, 16.
- [27] J.A.C. Weideman, Optimizing Talbot's contours for the inversion of the Laplace transform, *SIAM J. Numer. Anal.* 44 (6) (2006) 2342–2362.
- [28] J. Abate, W. Whitt, A unified framework for numerically inverting Laplace transforms, *INFORMS J. Comput.* 18 (4) (2006) 408–421.
- [29] Christian Engström, Stefano Giani, Luka Grubišić, A spectral projection based method for the numerical solution of wave equations with memory, *Appl. Math. Lett.* 127 (2022) Paper No. 107844, 9.